



## Aqueous metal ions adsorption by poly(ethylene glycol)-modified graphene oxide: surface area and surface chemistry effects

Jia-Ying Yang<sup>a,b,†</sup>, Bao-Yu Yue<sup>a,b,†</sup>, Jie Teng<sup>c</sup>, Xia Xu<sup>a,b</sup>, Xiao-Ru Zhao<sup>a,b</sup>, Xin-Yu Jiang<sup>a,b</sup>, Jin-Gang Yu<sup>a,b,\*</sup>, Fang-Liang Zhou<sup>d</sup>

<sup>a</sup>Key Laboratory of Hunan Province for Water Environment and Agriculture Product Safety, College of Chemistry and Chemical Engineering, Central South University, Changsha, Hunan 410083, China, Tel. +86 731 88879616; emails: yujg@csu.edu.cn (J.-G. Yu), 919620862@qq.com (J.-Y. Yang), 775498809@qq.com (B.-Y. Yue), 809703325@qq.com (X. Xu), 2808091270@qq.com (X.-R. Zhao), jiangxinyu@csu.edu.cn (X.-Y. Jiang)

<sup>b</sup>Hunan Provincial Key Laboratory of Efficient and Clean Utilization of Manganese Resources, College of Chemistry and Chemical Engineering, Central South University, Changsha, Hunan 410083, China

<sup>c</sup>College of Materials Science and Engineering, Hunan University, Changsha, Hunan 410082, China; email: tengjie@hnu.edu.cn

<sup>d</sup>Hunan Vocational College of Engineering, Changsha, Hunan 410151, China; email: yjgzfl@126.com

Received 5 March 2018; Accepted 19 October 2018

### ABSTRACT

To investigate the effects of oxygen contents and surface area of the adsorbents on their removal efficiencies, poly(ethylene glycol) (PEG) with various molecular masses (200, 2,000, and 20,000) modified graphene oxide (GO-PEG) composites were fabricated and used for the removal of Pb(II) from aqueous solutions. The morphologies, specific surface area, and surface functional groups of the GO-PEG composites were characterized by field-emission scanning electron microscopy, Brunauer–Emmett–Teller method, thermogravimetric and differential thermogravimetric analyses, Fourier-transform infrared spectroscopy, X-ray photoelectron spectroscopy, and Raman spectroscopy. Batch experiments were conducted to evaluate the effects of contact time, initial concentration, adsorbent dosage, and temperature on the adsorption efficiencies of the adsorbents. The experimental data indicated that the adsorption of Pb(II) onto GO-PEG composites fitted well to the pseudo-second-order kinetic model and the Langmuir isotherm model. Thermodynamic studies indicated that the adsorption was a spontaneous and endothermic process. The obtained GO-PEG (200), GO-PEG (2000), and GO-PEG (20000) composites exhibited the maximum adsorption capacities of 204.50, 72.73, and 196.46 mg g<sup>-1</sup> toward Pb(II), respectively. The higher adsorption capability of GO-PEG (200) toward Pb(II) could be attributed to its relatively higher oxygen content and larger SSA. The adsorption capacities of GO-PEG (200) toward other metal ions including Cu(II), Cd(II), Mn(II), Er(III), and Y(III) were 48.04, 80.48, 36.1, 23.1, and 12.2 mg g<sup>-1</sup>, respectively.

**Keywords:** Poly(ethylene glycol); Graphene oxide; Metal ions; Adsorption; Oxygen content; Surface area

### 1. Introduction

Water contaminations caused by persistent organic pollutants and heavy metals have threatened the balance of nature, the global sustainability, the biodiversity, and the human health [1–6]. Various treatment methods

including coagulation [7], chemical oxidation [8], photo-degradation [9,10], membrane separation [11], and adsorption [12–15] have been generally developed for the water restoration. Adsorption technique has been considered as one of the most important and highly efficient methods for

\* Corresponding author.

† Authors contributed equally to this work.

the treatment of wastewater due to its advantages such as easy implementation, low cost, and high efficiency. Effective adsorbents with strong affinity and high loading capacities for the contaminants are urgently needed and have been deeply investigated [1–3,12–15].

Due to their high specific surface area (SSA), abundant surface functional groups, porous structures, and excellent hydrothermal stability, carbon-based nanomaterials including graphene, carbon nanotubes, and fullerene have been widely employed as highly efficient adsorbents. As a member of nano-carbon derivatives, graphene oxide (GO) has shown a strong propensity to interact with positively charged species such as metal ions and cationic dyes due to its high theoretical surface area, extensive electron delocalization, good chelating ability, and abundant adsorption sites [16,17]. However, GO suffers a separation troubling in adsorption technique due to its better dispersion ability in aqueous solutions [18–21]. To improve the separation possibilities and enhance the adsorption capacities of GO-based adsorbents, there has been an increasing interest on the exploiting of novel covalent and noncovalent functionalized GO composites. Chelating groups including carbonyl ( $-C=O$ ), diol, hydroxyl ( $-OH$ ), thiol ( $-SH$ ), carboxyl ( $-COOH$ ), and amino ( $-NH_2$ ) have been considered to be beneficial to their adsorption efficiencies toward metal ions. For example, pyridine covalently modified GO composite showed an increased adsorption capacity of  $119.6 \text{ mg g}^{-1}$  toward  $\text{Cu(II)}$  due to the introduced nitrogen contents [22], and *N*-(trimethoxysilylpropyl) ethylenediamine triacetic acid-modified GO also exhibited higher adsorption capacity toward  $\text{Pb(II)}$  ( $479 \pm 46 \text{ mg g}^{-1}$ ) [23].

Poly(ethylene glycol) (PEG), a linear or branched poly-ether with nontoxic and non-immunogenic properties, is usually prepared through the ring-opening polymerization of ethylene oxide [24]. As one of the low-cost polymers, which are extensively used in pharmaceutical industry and tissue culture, PEG is soluble in water and biocompatible [25]. Carbon nanomaterials modified with PEG have been investigated, and the obtained nanocarbon-based composites were used as controlled release drug delivery and gene transfection carriers [26]. For example, hybrid PEG functionalized GO or reduced GO materials can be well dispersed in water and nonpolar/nonprotic solvents [27], which could be used for intracellular drug delivery [28,29] due to their relatively high cytocompatibility [30].

To generate more oxygen species on the surface of GO, herein, three kinds of PEG with different molecular masses were used as the modification reagents. The adsorption capacities of PEG-decorated GO (GO-PEG) composites toward metal ions were investigated. The effects of various parameters including initial metal ion concentration ( $10\text{--}90 \text{ mg L}^{-1}$ ), contact time ( $5\text{--}120 \text{ min}$ ), temperature ( $25^\circ\text{C}\text{--}45^\circ\text{C}$ ), and molecular masses of PEG were studied in detail. The adsorption kinetics, isotherm, and thermodynamics were also explored.

## 2. Materials and methods

### 2.1. Materials

Flake graphite (99.90%) was obtained from Tianjin Kermel Chemical Reagent Development Center (Tianjin, China). Lead nitrate (AR) was obtained from Xilong Chemical Co., Ltd.

(Guangdong, China). Sulfuric acid ( $\text{H}_2\text{SO}_4$ , 98%), phosphoric acid ( $\text{H}_3\text{PO}_4$ , 85%), hydrogen peroxide ( $\text{H}_2\text{O}_2$ , 30%), hydrochloric acid (HCl, 37%), and PEG of different molecular weights (Mw 200, 2,000, and 20,000  $\text{g mol}^{-1}$ ; AR) were purchased from Sinopharm Chemical Reagent Beijing Co., Ltd. (Shanghai, China). *N,N*-dimethyl formamide (DMF; AR), yttrium chloride heptahydrate ( $\text{YCl}_3 \cdot 7\text{H}_2\text{O}$ ; 99.90 wt%), and erbium chloride hexahydrate ( $\text{ErCl}_3 \cdot 6\text{H}_2\text{O}$ ; 99.90 wt%) were supplied by Tianjin Fuqi Chemical Co., Ltd. (Tianjin, China). Sodium hydride (NaH, 60% dispersion in mineral oil) was obtained from Shanghai Aladdin Biochemical Technology Co., Ltd. (Shanghai, China).

### 2.2. Preparation of GO

GO was prepared by the improved Hummers' method previously reported [31,32]. Flake graphite (0.3 g) and  $\text{KMnO}_4$  (1.5 g) were added in a round-bottom flask which was cooled in an ice-water bath. A mixture of concentrated  $\text{H}_2\text{SO}_4/\text{H}_3\text{PO}_4$  (40 mL;  $V/V = 9:1$ ) was slowly added into the mixture under vigorous stirring. The reaction was then constantly stirred at  $50^\circ\text{C}$  for another 12 h. After that, the reaction mixture was naturally cooled to room temperature, then poured into a solution of ice water (40 mL) and 30%  $\text{H}_2\text{O}_2$  (3 mL) until no more bubbles appeared. Finally, the obtained mixture was rinsed repeatedly with ultrapure water and centrifuged at 10,000 rpm until the pH of the supernatant was neutral. After that, the solid residue was dispersed in deionized water by ultrasonication, and freeze-dried at  $-50^\circ\text{C}$  for 48 h, then stored in a desiccator for further use.

### 2.3. Preparation of GO-PEG composites

2.0 g of NaH (60% dispersion in mineral oil) was suspended in anhydrous DMF (10 mL) under strictly water-free and oxygen-free conditions. A solution of PEG (4.0 g) (with different molecular weights of 200, 2,000, or 20,000  $\text{g mol}^{-1}$ ) and anhydrous DMF (40 mL) was added dropwise to the mixture under stirring. After the reaction was heated to  $50^\circ\text{C}$  for 3 h, 0.4 g of GO was added into the suspension and reacted at  $80^\circ\text{C}$  for 30 h. The resultant product was added into 20 mL of 0.1 M HCl for 24 h, and filtered, then rinsed repeatedly with ethanol and deionized water, finally freeze-dried to obtain PEG functionalized GO (marked as GO-PEG [200], GO-PEG [2000], and GO-PEG [20000], respectively) for further use.

### 2.4. Characterization of GO and its composites

The morphologies of GO and GO-PEG composites were characterized by a field-emission scanning electron microscopy (FE-SEM) using a MIRA3 TESCAN electron microscope (TESCAN, UK). Raman spectra were recorded on a micro-Raman spectrometer (Ramascope-2000, Renishaw, Gloucestershire, UK) with a laser excitation wavelength of 514.5 nm. Fourier-transform infrared (FT-IR) spectra of the samples were recorded on a Nicolet-Avatar360 FT-IR spectrometer (Thermo Nicolet Corporation, Madison, WI, USA). SSA measurements of the GO-PEG composites were carried out on a Kubo-X1000 analyzer (Beijing Builder Electronic Technology Co., Ltd., China) by the Brunauer–Emmett–Teller

(BET) nitrogen ( $N_2$ ) adsorption–desorption method at 77 K. Thermogravimetric and differential thermogravimetric (TG-DTG) analyses were conducted on a TA instruments DSC 2910 (TA instruments Inc., Wilmington, DE, USA) over a temperature range from room temperature to 1,000°C with a heating rate of 10°C min<sup>-1</sup> in argon (Ar) atmosphere. X-ray photoelectron spectroscopy (XPS) data were collected on a PHI-5000C ESCA system (PerkinElmer, MA, USA) with Al K $\alpha$  X-rays operated at 250 W.

### 2.5. Batch sorption experiments

Batch sorption experiments were carried out to study the sorption performances of Pb(II) on GO-PEG (200, 2000, and 20000) composites. The sorption capacities of various GO-PEG composites (5.0 mg) toward Pb(II) were investigated at three different temperatures of 298, 308, and 318 K, respectively. The condition parameters including initial Pb(II) concentrations (10–120 mg L<sup>-1</sup>), pH values (1.0–7.0), and contact time (5–120 min) were investigated. The adsorption kinetics, isotherms, and thermodynamics were also studied. Samples were withdrawn from the mixture at certain time intervals, which were filtered through a 0.45- $\mu$ m filter membrane, and then Pb(II) concentrations were determined by an inductively coupled plasma-optical emission spectroscopy. The adsorption capacity and removal efficiency of the GO-PEG (200, 2000, and 20000) composites could be calculated using the following equations:

$$q_e = (C_0 - C_e) \times V / m \quad (1)$$

$$R(\%) = (C_0 - C_e) / C_0 \times 100\% \quad (2)$$

where  $C_0$  and  $C_e$  (mg L<sup>-1</sup>) represent the initial and residual Pb(II) concentrations, respectively;  $V$  (L) represents the volume of Pb(II) solution;  $m$  (g) represents the mass of dry sorbent;  $q_e$  (mg g<sup>-1</sup>) is the equilibrium adsorption capacity of the adsorbent; and  $R$  (%) is the removal efficiency of the adsorbent toward Pb(II).

## 3. Results and discussion

### 3.1. Characterization

$N_2$  adsorption–desorption measurements were carried out to quantitatively analyze the SSA of the GO-PEG composites. Adsorption–desorption isotherm curves of the samples are displayed in Fig. 1. The three typical type-III isotherms of the GO-PEG composites exhibited a gradual increase in  $N_2$  adsorption with increasing  $p/p_0$ . The SSA of GO-PEG (200), GO-PEG (2000), and GO-PEG (20000) calculated by the BET method were 126.0472, 40.8159, and 39.4487 m<sup>2</sup> g<sup>-1</sup>, respectively. It is obvious that the GO-PEG (200) possesses the highest SSA among the three GO-based composites.

The differential thermal-thermogravimetric analysis (DT-TGA) and differential thermal differential thermogravimetric (DT-DTG) analyses of PEG-200, GO-PEG (200), PEG-2000, GO-PEG (2000), PEG-20000, and GO-PEG (20000) in argon (Ar) atmosphere at a heating rate of 10 K min<sup>-1</sup> were carried out. To determine the effect of chemical modification

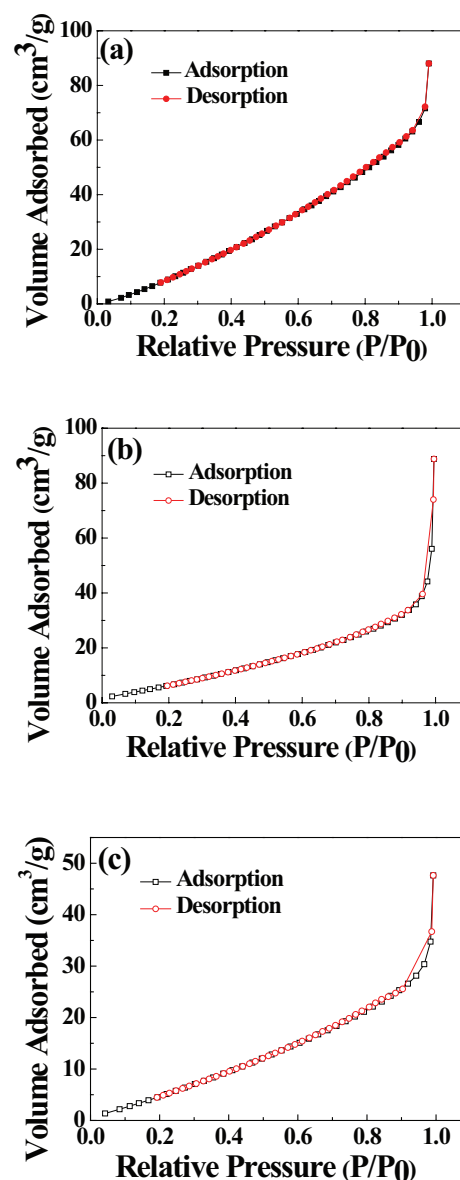


Fig. 1. The  $N_2$  adsorption–desorption isotherm loops of the samples: (a) GO-PEG (200), (b) GO-PEG (2000), and (c) GO-PEG (20000).

on thermal stability of the GO-PEG composites, the TG-DTG analyses were also carried out. As shown in Fig. 2, the weight losses of GO-PEG (200), GO-PEG (2000), and GO-PEG (20000) below 100°C which are related to the physically adsorbed water are 7.05, 7.27, and 7.89 wt%, respectively. The second weight loss (18.77 wt%) of GO-PEG (200) occurred in the temperature region of 342.32°C–807.46°C corresponded to thermal decomposition of grafted PEG-200. While the second weight loss (25.35 wt%) of GO-PEG (2000) occurred in the temperature region of 371.51°C–660.48°C, and the second weight loss (63.02 wt%) of GO-PEG (20000) occurred in the temperature region of 304.14°C–597.10°C.

In order to identify the surface functional groups, FT-IR spectra of the as-prepared GO, GO-PEG composites, and GO-PEG (200)-adsorbed Pb(II) were recorded (Fig. 3).

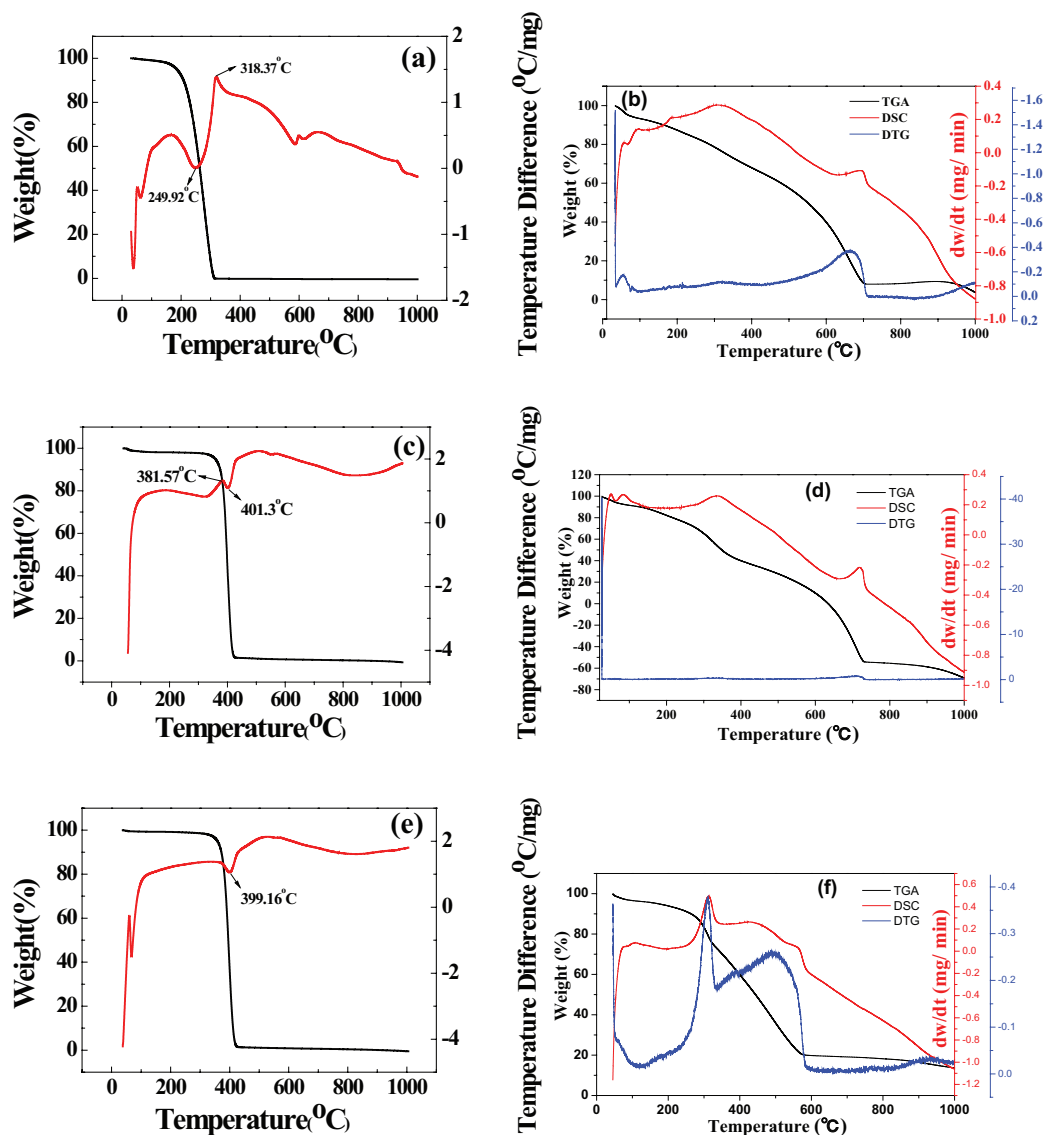


Fig. 2. DT-TGA and DT-DTG analyses of the samples: (a) PEG-200, (b) GO-PEG (200), (c) PEG-2000, (d) GO-PEG (2000), (e) PEG-20000, and (f) GO-PEG (20000).

As shown in Fig. 3(a), the absorption peak at  $3,402\text{ cm}^{-1}$  corresponds to the stretching vibration of hydroxy group ( $-\text{OH}$ ); the peak appeared at  $1,620\text{ cm}^{-1}$  corresponds to the stretching vibration of carbon-carbon double ( $\text{C}=\text{C}$ ) bond; the absorption peak at  $1,734\text{ cm}^{-1}$  is assigned to the stretching vibration of carboxyl group ( $\text{C}=\text{O}$ ); the peaks at  $1,141$  and  $1,114\text{ cm}^{-1}$  can be assigned to carbon-oxygen ( $\text{C}-\text{O}$ ) and carbon-oxygen-carbon ( $\text{C}-\text{O}-\text{C}$ ) stretching vibrations. The FT-IR spectra of GO-PEG (200), GO-PEG (2000), and GO-PEG (20000) were also obtained (Fig. 3(b)–(d)). All the spectra showed a common broad peak of  $-\text{OH}$  at  $3,445\text{--}3,430\text{ cm}^{-1}$ . While the absorption peaks of  $\text{C}=\text{O}$  bond shifted to  $1,715\text{--}1,700\text{ cm}^{-1}$ . What is more is that the peaks at  $1,245\text{--}1,210\text{ cm}^{-1}$  of  $\text{C}-\text{O}$  bonds and the peaks at  $1,169$ ,  $1,104$ , and  $1,088\text{ cm}^{-1}$  of  $\text{C}-\text{O}-\text{C}$  bonds are still presented. After adsorption of  $\text{Pb}(\text{II})$ , the absorption peak of  $\text{C}=\text{O}$  shifted to low wavenumber, indicating metal coordination was involved in the adsorption (Fig. 3(e)).

Raman spectroscopy is a powerful and sensitive tool for the characterization of graphene-based materials because of the high Raman intensities generated by the conjugated  $\text{C}=\text{C}$  bonds [33]. Fig. 3(f) shows the Raman spectra of GO, GO-PEG (200), GO-PEG (2000), and GO-PEG (20000). As can be seen, the two characteristic peaks at  $1,330$  and  $1,588\text{ cm}^{-1}$  which belong to the disorder band caused by the graphite edges and the in-phase vibration of the graphite lattice (G band), respectively [33], are presented for GO, GO-PEG (200), GO-PEG (2000), and GO-PEG (20000). The intensity ratio of the D band and G band ( $I_D/I_G$ ) indicated the density of structural defects on the surface of graphene-based composites. The  $I_D/I_G$  of the samples increased obviously for GO-PEG (200) ( $I_D/I_G = 1.23$ ), GO-PEG (2000) ( $I_D/I_G = 1.28$ ), and GO-PEG (20000) ( $I_D/I_G = 1.37$ ) compared with that of GO ( $I_D/I_G = 0.79$ ), indicating the presence of more defects due to the introduction of  $\text{sp}^3$ -hybridized oxygen-containing groups.

To demonstrate the morphologies of the samples, SEM characterization was carried out, and the obtained SEM images are shown in Fig. 4. Unlike the very smooth surface with fracture edges and layered structure of GO (Fig. 4(a)), multilayer stack structures could be observed in the GO-PEG composites (Figs. 4(b)–(d)). Due to the interactions between GO-PEG layers and the resulted agglomeration, thickened and wrinkled structures of the GO-PEG composites with rolled-up edges emerged. As shown in Table 1, the chemical compositions of the GO-based samples were analyzed by energy dispersive X-ray spectroscopy (EDS). The oxygen content in the samples gradually increased with an increase in the molecular mass of PEG.

### 3.2. Adsorption of Pb(II) onto GO-PEG: effects of the conditions, adsorption kinetics, pH values, thermodynamics, and isotherms

#### 3.2.1. Effects of contact time

The effects of contact time on the adsorption of Pb(II) by GO-PEG were investigated. As presented in Fig. 5, the adsorption of Pb(II) on the GO-PEG composites slowly increases

within 20 min, and equilibrium is reached after 30 min. The adsorption capacities of GO-PEG (200), GO-PEG (2000), and GO-PEG (20000) toward Pb(II) were 232.87, 100.56, and 175.72 mg g<sup>-1</sup>, respectively. GO-PEG (200) possesses the highest adsorption capacity due to its relatively larger SSA (Fig. 1). While GO-PEG (20000) possesses higher adsorption capacity than GO-PEG (2000), indicating the presence of more oxygen groups is beneficial to the adsorption when the adsorbents possess similar SSA (Fig. 1; Table 1).

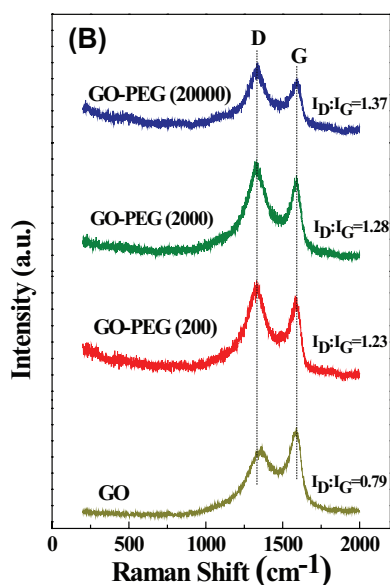
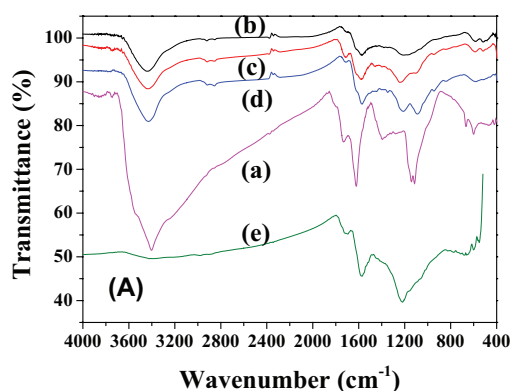


Fig. 3. Spectral curves of the samples: (A) FT-IR (a) GO, (b) GO-PEG (200), (c) GO-PEG (2000), (d) GO-PEG (20000), and (e) GO-PEG (200)-adsorbed Pb(II); and (B) Raman spectra.

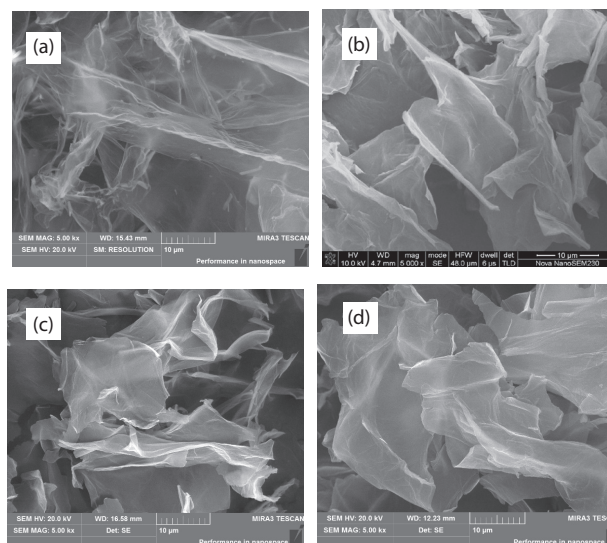


Fig. 4. SEM images of the samples: (a) GO, (b) GO-PEG (200), (c) GO-PEG (2000), and (d) GO-PEG (20000). Scale bars are 10 μm.

Table 1  
EDS data of the GO-based sorbents

Samples	C (wt%)	O (wt%)
GO	83.90	16.10
GO-PEG (200)	70.84	29.16
GO-PEG (2000)	67.79	32.21
GO-PEG (20000)	63.95	36.05

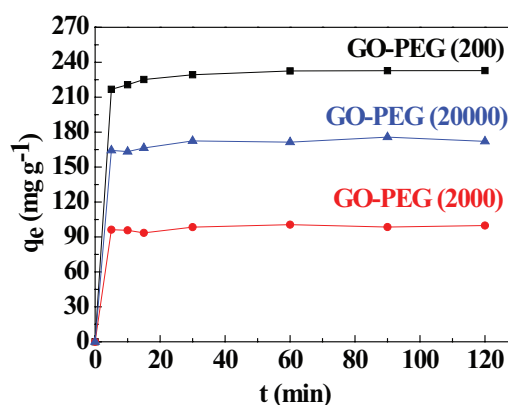


Fig. 5. Effects of contact time on the removal of Pb(II) by GO-PEG ( $C_0 = 50 \text{ mg L}^{-1}$ ,  $m = 5 \text{ mg}$ , and  $T = 298 \text{ K}$ ).

### 3.2.2. Effects of initial Pb(II) concentration

Series of adsorption experiments were undertaken to investigate the effects of the initial Pb(II) concentration (10–90 mg L<sup>-1</sup>) on the removal rate of GO-PEG composites. As shown in Fig. 6, the GO-PEG (200) and GO-PEG (20000) exhibited sharply enhanced adsorption capacities at a low concentration Pb(II), and then adsorption slowed down and gently reached the maximum in later stages because a large number of available surface sites may be largely occupied in the initial stages.

### 3.2.3. Effects of pH

The surface charge on an adsorbent and the existing ion species would be affected by changing the solution pH value, which would then affect the adsorption properties of GO-PEG composites toward metal ions. To observe pH values on the performance of GO-PEG composites toward Pb(II), the initial pH values of all solutions were adjusted in the range of 1.0–7.0 using standardized hydrochloric acid (HCl, 1 mol L<sup>-1</sup>) and sodium hydroxide (NaOH, 1 mol L<sup>-1</sup>) solution because Pb(II) would form a precipitate at high pH value of over 8.4 due to the solubility product constant of Pb(OH)<sub>2</sub> ( $K_{sp} = 1.2 \times 10^{-15}$ ). Obviously, the adsorption capacities of GO-PEG composites toward Pb(II) increased with an increase of pH values, indicating the existence of adsorption competition between Pb(II) and hydrogen ion (H<sup>+</sup>) (Fig. 7).

### 3.2.4. Effects of temperature on Pb(II) sorption and adsorption thermodynamics

Changes of Gibbs free energy ( $\Delta G^\circ$ , KJ mol<sup>-1</sup>), enthalpy ( $\Delta H^\circ$ , KJ mol<sup>-1</sup>), entropy ( $\Delta S^\circ$ , J K<sup>-1</sup> mol<sup>-1</sup>), and other thermodynamic parameters were determined using the following equations:

$$K_d = \frac{a_s}{a_e} = \frac{\gamma_s C_s}{\gamma_e C_e} \quad (3)$$

$$\Delta G^\circ = -RT \ln K_d \quad (4)$$

$$\Delta G^\circ = \Delta H^\circ - T\Delta S^\circ \quad (5)$$

where  $K_d$  is the thermodynamic equilibrium constant;  $T$  (K) is the absolute temperature of the solution;  $R$  is the universal gas constant (8.314 J mol<sup>-1</sup> K<sup>-1</sup>);  $a_s$  and  $a_e$  are the activity of adsorbed Pb(II) and the activity of Pb(II) in solution at equilibrium, respectively;  $\gamma_s$  and  $\gamma_e$  are the activity coefficient

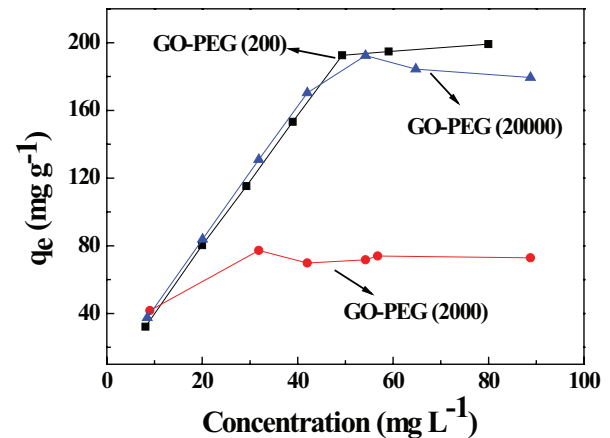


Fig. 6. Effects of initial Pb(II) concentrations on adsorption capacities of GO-PEG composites (adsorbent dosage = 5 mg/20 mL and contact time = 120 min).

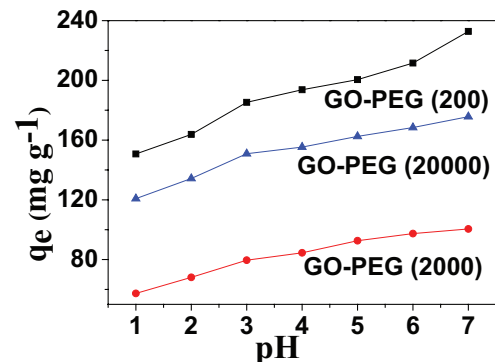


Fig. 7. Effects of initial pH on the adsorption of Pb(II) onto GO-PEG composites (adsorbent dosage = 5 mg/20 mL,  $C_0 = 50$  mg L<sup>-1</sup>, and contact time = 120 min).

of adsorbed Pb(II) and the activity coefficient of Pb(II) in equilibrium solution, respectively; and  $C_s$  denotes the amount of Pb(II) adsorbed on the adsorbent (mg g<sup>-1</sup>).

As listed in Table 2, the negative values of  $\Delta G^\circ$  revealed that the adsorption process is spontaneous in the temperature range of 298–318 K. The low and positive  $\Delta H^\circ$  values (<20 KJ mol<sup>-1</sup>) also indicated that the mechanism is physisorption and the adsorption is endothermic. The absolute value of  $\Delta G^\circ$  increased with an increase of temperature, indicating that the reaction temperature is a major driving force, and an endothermic sorption process can again be proved. The positive  $\Delta S^\circ$  values indicated the randomness at the solid/solution interfaces increased during the Pb(II) sorption onto the GO-PEG composites.

Table 2

Adsorption thermodynamic parameters of Pb(II) onto GO-PEG composites at different temperatures

Adsorbent	$\Delta G^\circ_{298}$ (KJ mol <sup>-1</sup> )	$\Delta G^\circ_{308}$ (KJ mol <sup>-1</sup> )	$\Delta G^\circ_{318}$ (KJ mol <sup>-1</sup> )	$\Delta H^\circ$ (KJ mol <sup>-1</sup> )	$\Delta S^\circ$ (J K <sup>-1</sup> mol <sup>-1</sup> )	$R^2$
GO-PEG (200)	-7.261	-7.984	-8.708	14.296	72.337	0.999
GO-PEG (2000)	-2.637	-3.204	-3.772	14.273	56.744	0.994
GO-PEG (20000)	-3.486	-3.733	-3.981	3.892	24.758	0.999

### 3.2.5. Adsorption kinetics

To deeply explore the adsorption process, the experimental data of the adsorption process were analyzed using pseudo-first-order model, pseudo-second-order model, and intraparticle diffusion model, respectively. Equations representing these models are listed as follows.

The pseudo-first-order equation is expressed as follows:

$$\ln(q_e - q_t) = \ln q_e - k_1 t \tag{6}$$

The pseudo-second-order equation is expressed as follows:

$$\frac{t}{q_t} = \frac{1}{k_2 q_e^2} + \frac{1}{q_e} t \tag{7}$$

The Intra particle diffusion equation is expressed as follows:

$$q_t = k_{dif} t^{1/2} + c \tag{8}$$

where  $k_1$  ( $\text{min}^{-1}$ ) and  $k_2$  ( $\text{mg min g}^{-1}$ ) are the adsorption rate coefficient of pseudo-first-order and pseudo-second-order kinetic models, respectively;  $q_e$  and  $q_t$  ( $\text{mg g}^{-1}$ ) are the values of the amount of Pb(II) adsorbed per unit mass at equilibrium and instant of time  $t$  (min), respectively; and  $k_{dif}$  ( $\text{mg g}^{-1} \text{min}^{1/2}$ ) is the intraparticle diffusion rate constant.

All the kinetic data were calculated (Fig. 8), fitted to the above three equations and tabulated in Table 3. As can be seen from the coefficient of determination ( $R^2$ ), it is obvious that pseudo-second-order model provided a better fit to the obtained data. In addition, the  $q_e$  value calculated by the pseudo-second-order model was also more consistent to the experimental data. Therefore, it could be concluded that the adsorption kinetics of Pb(II) onto GO-PEG composites could be described by the pseudo-second-order reaction model.

### 3.2.6. Adsorption isotherms

The adsorption isotherm could provide the qualitative information about the adsorption capacity of the adsorbent and the distribution of the adsorbate among the solid adsorbent and the liquid phase at equilibrium [34]. To simulate the adsorption isotherms of Pb(II) onto the GO-PEG composites, Langmuir (Eq. (9)) and Freundlich (Eq. (10)) isotherm models were used for analyzing the experimental data, respectively.

$$\frac{c_e}{q_e} = \frac{1}{b q_m} + \frac{c_e}{q_m} \tag{9}$$

$$\ln q_e = \ln K_F + \frac{1}{n} \ln C_e \tag{10}$$

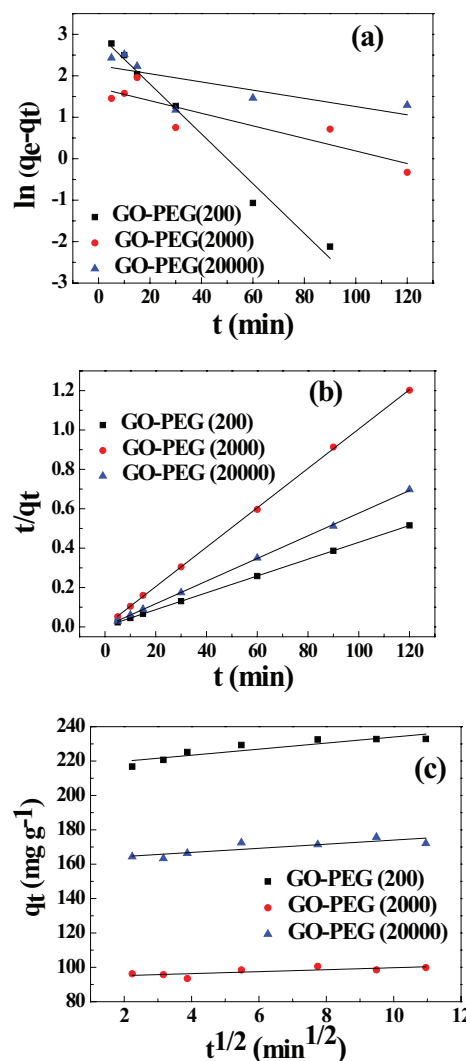


Fig. 8. The plots for the adsorption of Pb(II) onto GO-PEG composites: (a) pseudo-first-order kinetics model, (b) pseudo-second-order kinetics model, and (c) intraparticle diffusion model.

Table 3  
Parameters of different kinetic models for the adsorption of Pb(II) onto the GO-PEG sorbents

Adsorbent	Pseudo-first-order model			Pseudo-second-order model			Intraparticle diffusion model	
	$k_1$	$q_e$	$R^2$	$k_2$	$q_e$	$R^2$	$k_{dif}$	$R^2$
GO-PEG (200)	0.06004	20.11	0.9804	0.00818	234.19	0.9999	1.76505	0.7934
GO-PEG (2000)	0.01516	5.49	0.7417	0.02096	100.00	0.9998	0.57243	0.4976
GO-PEG (20000)	0.00990	9.47	0.3909	0.01328	173.91	0.9997	1.19748	0.6689

where  $q_e$  and  $q_m$  ( $\text{mg g}^{-1}$ ) are the equilibrium amount of adsorbate on adsorbent and the maximum adsorption capacity of the adsorbent, respectively;  $C_e$  ( $\text{mg L}^{-1}$ ) represents the Pb(II) concentration at equilibrium;  $b$  ( $\text{L mg}^{-1}$ ) is the Langmuir constant related to the adsorption energy; and  $K_F$  and  $1/n$  represent the Freundlich constants related to the adsorption capacity and the adsorption intensity, respectively.

The adsorption of Pb(II) onto GO-PEG composites was investigated with varying initial concentrations (10–90  $\text{mg L}^{-1}$ ) at three different temperatures (298, 308, and 318 K). The adsorption isotherm parameters of Pb(II) onto GO-PEG sorbents are shown in Fig. 9, and the parameters calculated from the two isotherm models are listed in Table 4. From the  $R^2$  values, it is obvious that the adsorption data are better fitted to the Langmuir isotherm model ( $R^2 > 0.98$ ), assuming monolayer adsorption occurs at the finite or fixed number of definite localized sites [47]. The results are highly in agreement with the above adsorption kinetics analysis. Furthermore, GO-PEG (200) showed observably

higher  $q_m$  (204.5  $\text{mg g}^{-1}$ ) for Pb(II) due to its larger SSA and higher amount of oxygen-containing functional groups.

To verify the practicability of the developed GO-PEG adsorbent, the removal of Pb(II) from Xiangjiang River water (Changsha, China) was studied. The removal rate of GO-PEG (200) and GO-PEG (20000) for the Pb(II) solution with low-concentration (50  $\text{mg L}^{-1}$ ) was up to 100% in 30 min. The adsorption performance of GO-PEG (200) Cu(II), Cd(II), Mn(II), Er(III), and Y(III) was also investigated, and the adsorption capacities were tested to be 48.04, 80.48, 36.1, 23.1, and 12.2  $\text{mg g}^{-1}$ , respectively.

### 3.2.7. Contrast experiments

The contrast of the Pb(II) adsorption capacities of GO-PEG composites with previously reported adsorbents is summarized in Table 5. It is obvious that some adsorbents including *Aspergillus oryzae* (HA) composited by peanut

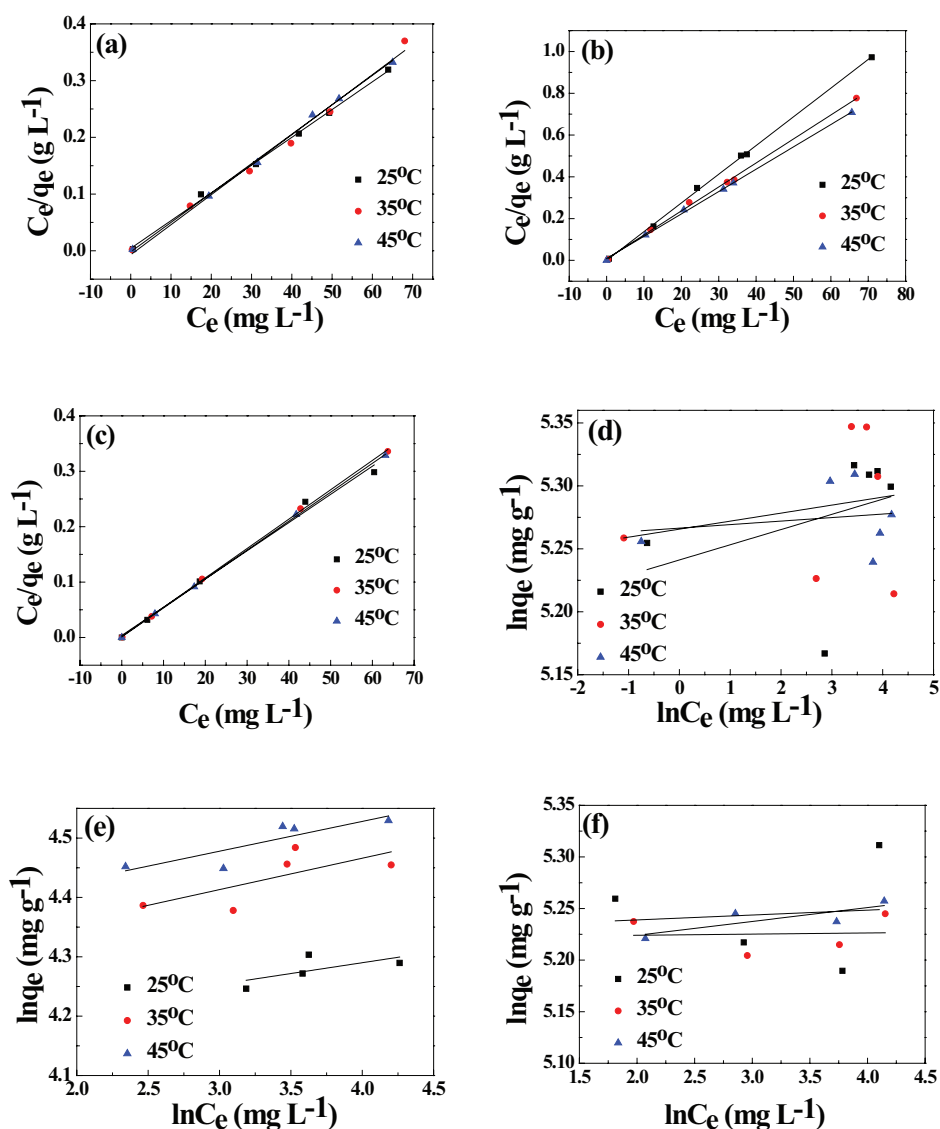


Fig. 9. The Langmuir model of Pb(II) on (a) GO-PEG (200), (b) GO-PEG (2000), (c) GO-PEG (20000) and the Freundlich model of Pb(II) on (d) GO-PEG (200), (e) GO-PEG (2000), and (f) GO-PEG (20000) at three different temperatures.

Table 4  
Calculated isotherm parameters of Pb(II) onto GO-PEG sorbents by Langmuir and Freundlich isotherm models

Adsorbent	Models	Parameters	298 K	308 K	318 K
GO-PEG (200)	Langmuir	$b$	1.1506	-0.7612	-2.7701
		$q_m$	204.50	189.04	193.05
		$R^2$	0.9972	0.9885	0.9982
	Freundlich	$K_F$	188.89	193.57	193.73
		$1/n$	0.0121	0.0064	0.0028
		$R^2$	0.1386	0.0458	0.0353
GO-PEG (2000)	Langmuir	$b$	-0.0248	1.6676	1.2876
		$q_m$	72.73	87.03	93.46
		$R^2$	0.9991	0.9981	0.9990
	Freundlich	$K_F$	63.07	70.43	75.74
		$1/n$	0.0364	0.0529	0.0502
		$R^2$	0.4291	0.5163	0.7489
GO-PEG (20000)	Langmuir	$b$	1.3683	3.3333	4.7455
		$q_m$	196.46	188.68	191.57
		$R^2$	0.9901	0.9994	0.9998
	Freundlich	$K_F$	186.69	185.27	180.74
		$1/n$	0.0047	0.0011	0.0135
		$R^2$	0.0084	0.0033	0.6706

Table 5  
A comparison of the maximum Pb(II) adsorption capacities of various adsorbents

Adsorbents	$q_m$ (mg g <sup>-1</sup> )	Reference
Peanut shell-HA	20.92	[35]
Millet chaff-HA	21.786	
CSB@Fe <sub>3</sub> O <sub>4</sub>	83.33	[36]
ox-MWCNT-Cl <sub>2</sub>	87.57	[12]
SY-m-SNPs	94.53	[37]
XG/GG	98.4	[38]
GO-TA	125.63	[39]
SAPL	130.2	[40]
nZVI/OBA	160.00	[41]
WHAC	118.8	[42]
Cross-linked GO	186.48	[43]
SMA	143.3	[44]
MDA@Fe <sub>3</sub> O <sub>4</sub>	333.3	[45]
Porous biosilica	120.4	[46]
GO-PEG (200)	204.50	This work
GO-PEG (2000)	72.73	
GO-PEG (20000)	196.46	

ox-MWCNT-Cl<sub>2</sub>, diiodocarbene functionalized oxidized multi-walled carbon nanotube.

shell (peanut shell-HA) or millet chaff (millet chaff-HA), sodium hypochlorite-modified starch nanoparticles (SY-m-SNPs), chitosan schiffs base@Fe<sub>3</sub>O<sub>4</sub> (CSB@Fe<sub>3</sub>O<sub>4</sub>), sulfuretted lignin (SAPL), tartaric acid-modified GO (GO-TA), activated carbon from water hyacinth (WHAC), polysaccharide mixes of xanthan gum, synthetic mineral adsorbent (SMA), and guar gum (XG/GG), zerovalent iron particles-modified

ostrich bone ash (nZVI/OBA), and melamine-based dendrimer amine-modified Fe<sub>3</sub>O<sub>4</sub> (MDA@Fe<sub>3</sub>O<sub>4</sub>) showed lower Pb(II) adsorption capacities than those of GO-PEG (200) and GO-PEG (20000), indicating the GO-PEG composites could be used as highly efficient adsorbents in removal of metal ions from aqueous solutions.

### 3.2.8. Adsorption mechanism of Pb(II) onto GO-PEG sorbents

The schematic representation of Pb(II) adsorption onto GO-PEG is shown in Fig. 10. First, PEG reacted with NaH to form alkoxide negative ion; second, a nucleophilic addition reaction and a ring-opening addition reaction occurred between the alkoxide negative ion and GO to generate the GO-PEG composite. Due to the abundant oxygen-containing groups (-C=O, -OH, and -COOH of GO and terminal -OH and C-O-C of PEG), it is easy for the formation of complexes between GO-PEG and Pb(II).

From FT-IR spectra (Fig. 4(e)), it is obvious that metal-oxygen coordination was involved in the adsorption because the absorption peak of C=O of the GO-PEG (200)-adsorbed Pb(II) shifted to low wavenumber (Fig. 4(e)). In addition, the chemical states of C, O, and Pb of GO-PEG (200)-adsorbed Pb(II) were also analyzed by XPS (Fig. 11(a)). It is obvious that there are C 1s, O 1s, and Pb 4f peaks in GO-PEG (200)-adsorbed Pb(II). The C 1s and O 1s spectra have been previously investigated in detail [24]. The C 1s spectra reveal four characteristic peaks at 284.5 eV (C=C), 284.9 eV (C-O), 285.4 eV (C=O), and 286.6 eV (O-C=O), respectively (Fig. 11(b)). And, the O 1s spectra reveal three characteristic peaks at 531.6 eV (C-O), 532.5 eV (C=O), and 533.7 eV (O-C=O), respectively (Fig. 11(c)). The Pb 4f spectra for the GO-PEG (200)-adsorbed Pb(II) showed two sets of 4f doublet peaks at 144.2/139.3 eV and 143.6/138.6 eV in accordance with the reference compounds of PbO and Pb(NO<sub>3</sub>)<sub>2</sub>

in the literature [48], indicating the presence of Pb(II) on the surface of the adsorbent through both direct physisorptions and Pb–O coordination interactions (Fig. 11(d)).

From previous characterization (Fig. 1), it is obvious that GO-PEG (200) possesses the highest BET SSA ( $126.0 \text{ m}^2 \text{ g}^{-1}$ ) which is almost three times as that of GO-PEG

(200) ( $40.8 \text{ m}^2 \text{ g}^{-1}$ ) or GO-PEG (20000) ( $39.4 \text{ m}^2 \text{ g}^{-1}$ ), indicating that better physical adsorption can be achieved by GO-PEG (200) composite. Additionally, the oxygen content in the samples gradually increased with an increase in the molecular mass of PEG from 200 to 20000, indicating that more active adsorption sites were formed on the surface of the

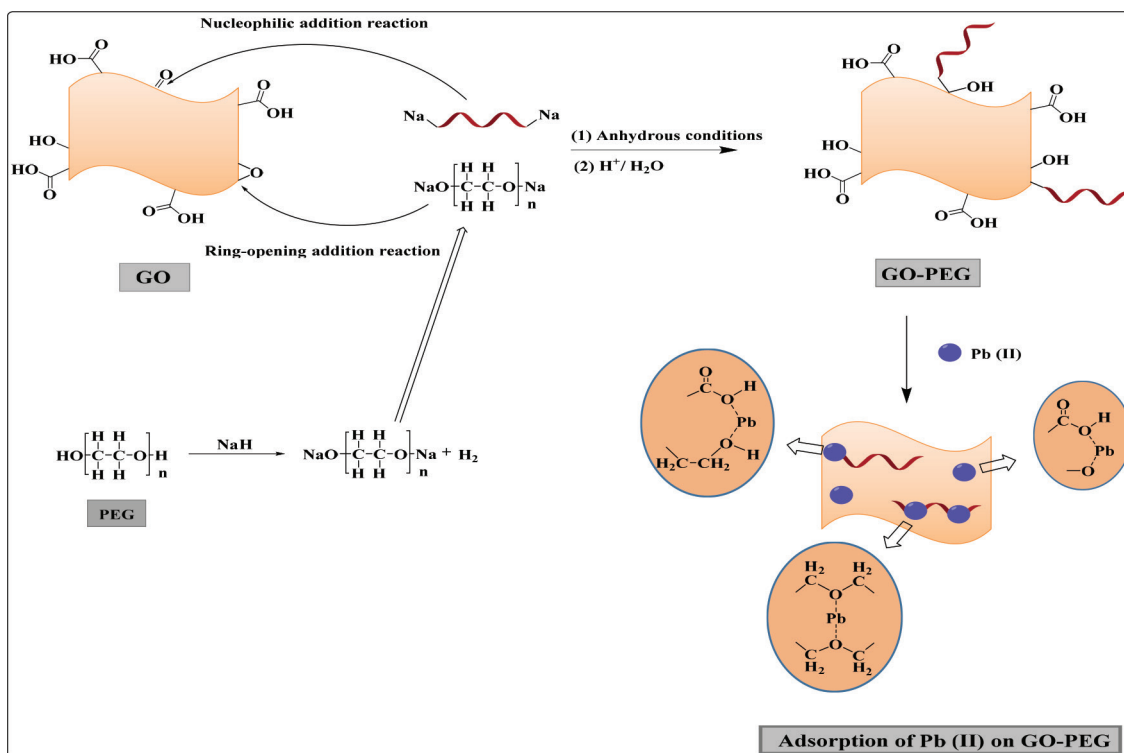


Fig. 10. Schematic representation of the Pb(II) adsorption onto GO-PEG sorbents.

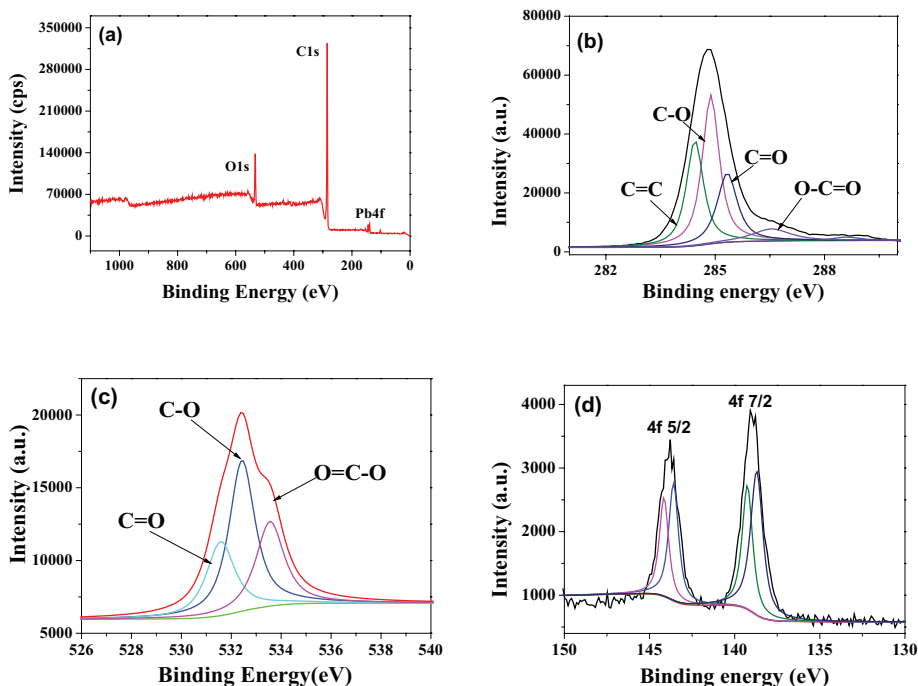


Fig. 11. XPS of GO-PEG (200)-adsorbed Pb(II): (a) full spectrum, (b) C 1s region, (c) O 1s region, and (d) Pb 4f region.

adsorbents. However, the differences observed at the oxygen content levels of the three adsorbents were minor. Therefore, physisorption dominates the reaction and GO-PEG (200) possesses the highest adsorption capacities for Pb(II). GO-PEG (2000) and GO-PEG (20000) possess almost the same SSA, while the latter possesses higher oxygen content. Therefore, GO-PEG (20000) showed relatively higher adsorption capacities for Pb(II) than that of GO-PEG (2000).

### 3.2.9. Regeneration of the adsorbents

The regeneration of an adsorbent is very important for its practical applications. The initial Pb(II) concentration and the amount of GO-PEG (200) were set to be 20 and 500 mg L<sup>-1</sup>, respectively. After the adsorption, the adsorbent was filtered from the solution and soaked in dilute nitric acid (HNO<sub>3</sub>, 0.1 mol L<sup>-1</sup>) for 4 h, then rinsed with deionized water for three times, and used for another adsorption. The adsorption efficiency of GO-PEG (200) approached 95% even after five successive cycles of adsorption–desorption.

## 4. Conclusion

To evaluate the effects of the SSA and the surface complexation groups of the adsorbents toward metal ions, GO-PEG (200), GO-PEG (2000), and GO-PEG (20000) were prepared by a nucleophilic addition reaction. The morphologies, surface functional groups, SSA, and chemical compositions of the GO-PEG sorbents were characterized by FE-SEM, BET, DT-TGA, FT-IR, XPS, and Raman spectra. By using Pb(II) as the model metal ion, the removal abilities of the GO-PEG sorbents toward metal ions were investigated. The adsorption conditions were optimized. The adsorption thermodynamics, kinetics, and isotherms were studied in detail. The maximum adsorption capacities of GO-PEG (200), GO-PEG (2000), and GO-PEG (20000) for Pb(II) reached 204.50, 72.73, and 196.46 mg g<sup>-1</sup>, respectively. The removal rate of GO-PEG (200) and GO-PEG (20000) for the Pb(II) solution with low-concentration (50 mg L<sup>-1</sup>) was up to 100% in 30 min. Both the SSA and the surface functional groups were found to greatly affect the adsorption performance of the adsorbents. The results could provide some references for the further researches in developing and researching novel highly efficient adsorbents.

## Acknowledgments

The financial supports from National Natural Science Foundation of China (Nos. 51674292, 21471163, 21571191, and 51574118), Provincial Natural Science Foundation of Hunan (No. 2016JJ1023), and Hunan Provincial Science and Technology Plan Project, China (Nos. 2018TP1003 and 2016TP1007) are greatly appreciated.

## References

- [1] L.Y. Chai, Q.W. Wang, Q.Z. Li, Z.H. Yang, Y.Y. Wang, Enhanced removal of Hg(II) from acidic aqueous solution using thiol-functionalized biomass, *Water Sci. Technol.*, 62 (2010) 2157–2166.
- [2] Q.Z. Li, L.Y. Chai, Z.H. Yang, Q.W. Wang, Y.Y. Wang, A comparative study of Ag(I) adsorption on raw and modified spent grain: kinetic and thermodynamic aspects, *Water Environ. Res.*, 82 (2010) 2290–2296.
- [3] Y.Y. Wang, B. Peng, Z.H. Yang, C.J. Tang, Y.H. Chen, Q. Liao, Y.P. Liao, Treatment of Cr(VI) contaminated water with *Pannonibacter phragmitetus* BB, *Environ. Earth Sci.*, 71 (2014) 4333–4339.
- [4] T. Wang, L.Y. Zhang, C.F. Li, W.C. Yang, T.T. Song, C.J. Tang, Y. Meng, S. Dai, H.Y. Wang, L.Y. Chai, J. Luo, Synthesis of core-shell magnetic Fe<sub>3</sub>O<sub>4</sub>@poly(m-phenylenediamine) particles for chromium reduction and adsorption, *Environ. Sci. Technol.*, 49 (2015) 5654–5662.
- [5] X. Xu, J. Zou, J. Teng, Q. Liu, X.Y. Jiang, F.P. Jiao, J.G. Yu, X.Q. Chen, Novel high-gluten flour physically cross-linked graphene oxide composites: hydrothermal fabrication and adsorption properties for rare earth ions, *Ecotox. Environ. Safe.*, 166 (2018) 1–10.
- [6] J.-Y. Yang, X.-Y. Jiang, F.-P. Jiao, J.-G. Yu, The oxygen-rich pentaerythritol modified multi-walled carbon nanotube as an efficient adsorbent for aqueous removal of alizarin yellow R and alizarin red S, *Appl. Surf. Sci.*, 436 (2018) 198–206.
- [7] C.A. Basha, M. Somasundaram, T. Kannadasan, C.W. Lee, Heavy metals removal from copper smelting effluent using electrochemical filter press cells, *Chem. Eng. J.*, 171 (2011) 563–571.
- [8] X. Liu, T. Zhao, H. Cheng, C. Zhu, S. Li, P. Cui, In-situ synthesis of nanomagnetites on poly(amidoamine)-modified graphite oxides and their novel catalytic performances towards the degradation of p-nitro aniline, *Appl. Surf. Sci.*, 327 (2015) 226–232.
- [9] V. Belgiorno, L. Rizzo, D. Fatta, C.D. Rocca, G. Lofrano, A. Nikolaou, V. Naddeo, S. Meric, Review on endocrine disrupting-emerging compounds in urban wastewater: occurrence and removal by photocatalysis and ultrasonic irradiation for wastewater reuse, *Desalination*, 215 (2007) 166–176.
- [10] J.-G. Yu, J. Zou, L.-L. Liu, X.-Y. Jiang, F.-P. Jiao, X.-Q. Chen, Preparation of TiO<sub>2</sub> based photocatalysts and their photocatalytic degradation properties for methylene blue, rhodamine B and methyl orange, *Desal. Wat. Treat.*, 81 (2017) 282–290.
- [11] H.R. Mortaheb, A. Zolfaghari, B. Mokhtarani, M.H. Amini, V. Mandanipour, Study on removal of cadmium by hybrid liquid membrane process, *J. Hazard. Mater.*, 177 (2010) 660–667.
- [12] J.-Y. Yang, X.-Y. Jiang, F.-P. Jiao, J.-G. Yu, X.-Q. Chen, Fabrication of diiodocarbene functionalized oxidized multi-walled carbon nanotube and its aqueous adsorption performance toward Pb(II), *Environ. Earth Sci.*, 76 (2017) 677.
- [13] Z.A. Wang, X.M. Zhang, X.W. Wu, J.-G. Yu, X.-Y. Jiang, Z.-L. Wu, X. Hao, Soluble starch functionalized graphene oxide as an efficient adsorbent for aqueous removal of Cd(II): the adsorption thermodynamic, kinetics and isotherms, *J. Sol-Gel Sci. Technol.*, 82 (2017) 440–449.
- [14] N. Chen, J. Teng, F.-P. Jiao, X.-Y. Jiang, X. Hao, J.-G. Yu, Preparation of triethanolamine functionalized carbon nanotube for aqueous removal of Pb(II), *Desal. Wat. Treat.*, 71 (2017) 191–200.
- [15] Y.J.O. Asencios, M.R. Sun-Kou, Synthesis of high-surface-area  $\gamma$ -Al<sub>2</sub>O<sub>3</sub> from aluminum scrap and its use for the adsorption of metals: Pb(II), Cd(II) and Zn(II), *Appl. Surf. Sci.*, 258 (2012) 10002–10011.
- [16] O. Moradi, V.K. Gupta, S. Agarwal, I. Tyagi, M. Asif, A.S.H. Makhlof, H. Sadegh, R. Shahryari-ghoshekandi, Characteristics and electrical conductivity of graphene and graphene oxide for adsorption of cationic dyes from liquids: kinetic and thermodynamic study, *J. Ind. Eng. Chem.*, 28 (2015) 294–301.
- [17] Y. Sun, X. Wang, W. Song, S. Lu, C. Chen, X. Wang, Mechanistic insights into the decontamination of Th(IV) on graphene oxide-based composites by EXAFS and modeling techniques, *Environ. Sci. Nano*, 4 (2017) 222–232.
- [18] Y. Sun, S. Yang, Y. Chen, C. Ding, W. Cheng, X. Wang, Adsorption and desorption of U(VI) on functionalized graphene oxides: a combined experimental and theoretical study, *Environ. Sci. Technol.*, 49 (2015) 4255–4262.
- [19] Y. Sun, Q. Wang, C. Chen, X. Tan, X. Wang, Interaction between Eu(III) and graphene oxide nanosheets investigated by batch and extended X-ray absorption fine structure spectroscopy and by modeling techniques, *Environ. Sci. Technol.*, 46 (2012) 6020–6027.

- [20] J. Zou, L.L. Huang, X.Y. Jiang, F.P. Jiao, J.G. Yu, Electrochemical behaviors and determination of rifampicin on graphene nanoplatelets modified glassy carbon electrode in sulfuric acid solution, *Desal. Wat. Treat.*, 120 (2018) 272–281.
- [21] Z.-H. Wang, J.-Y. Yang, X.-W. Wu, X.-Q. Chen, J.-G. Yu, Y.-P. Wu, Enhanced electrochemical performance of porous activated carbon by forming composite with graphene as high-performance supercapacitor electrode material, *J. Nanopart. Res.*, 19 (2017) 77.
- [22] Y. Guo, Z. Jia, M. Cao, Surface modification of graphene oxide by pyridine derivatives for copper(II) adsorption from aqueous solutions, *J. Ind. Eng. Chem.*, 53 (2017) 325–332.
- [23] C.J. Madadrang, H.Y. Kim, G. Gao, N. Wang, J. Zhu, H. Feng, M.L. Gorrng, M.L. Kasner, S. Hou, Adsorption behavior of EDTA-graphene oxide for Pb(II) removal, *ACS Appl. Mater. Interfaces*, 4 (2012) 1186–1193.
- [24] B.-Y. Yue, L.-Y. Yu, F.-P. Jiao, X.-Y. Jiang, J.-G. Yu, The fabrication of pentaerythritol pillared graphene oxide composite and its adsorption performance towards metal ions from aqueous solutions, *Desal. Wat. Treat.*, 102 (2018) 124–133.
- [25] R. Bhattacharyya, S.K. Ray, Removal of congo red and methyl violet from water using nano clay filled composite hydrogels of poly acrylic acid and polyethylene glycol, *Chem. Eng. J.*, 260 (2015) 269–283.
- [26] S. Stankovich, D.A. Dikin, G.H.B. Dommett, K.M. Kohlhaas, E.J. Zimney, E.A. Stach, R.D. Piner, S.T. Nguyen, R.S. Ruoff, Graphene-based composite materials, *Nature*, 442 (2006) 282–286.
- [27] S. Zhang, P. Xiong, X. Yang, X. Wang, Novel PEG functionalized graphene nanosheets: enhancement of dispersibility and thermal stability, *Nanoscale*, 3 (2011) 2169–2174.
- [28] X. Sun, Z. Liu, K. Welsher, J.T. Robinson, A. Goodwin, S. Zaric, H. Dai, Nano-graphene oxide for cellular imaging and drug delivery, *Nano Res.*, 1 (2008) 203–212.
- [29] H. Wen, C. Dong, H. Dong, A. Shen, W. Xia, X. Cai, Y. Song, X. Li, Y. Li, D. Shi, Engineered redox-responsive PEG detachment mechanism in PEGylated nano-graphene oxide for intracellular drug delivery, *Small*, 8 (2012) 760–769.
- [30] M. Wojtoniszak, X. Chen, R.J. Kalenczuk, A. Wajda, J. Lapczuk, M. Kurzawski, M. Drozdziak, P.K. Chu, E. Borowiak-Palen, Synthesis, dispersion, and cytocompatibility of graphene oxide and reduced graphene oxide, *Colloids Surf., B*, 89 (2012) 79–85.
- [31] X. Xu, X.-Y. Jiang, F.-P. Jiao, X.-Q. Chen, J.G. Yu, Tunable assembly of porous three-dimensional graphene oxide-corn zein composites with strong mechanical properties for adsorption of rare earth elements, *J. Taiwan Inst. Chem. Eng.*, 85 (2018) 106–114.
- [32] J. Teng, X. Zeng, X. Xu, J.-G. Yu, Assembly of a novel porous 3D graphene oxide-starch architecture by a facile hydrothermal method and its adsorption properties toward metal ions, *Mater. Lett.*, 214 (2018) 31–33.
- [33] K.N. Kudin, B. Ozbas, H.C. Schniepp, R.K. Prud'homme, I.A. Aksay, R. Car, Raman spectra of graphite oxide and functionalized graphene sheets, *Nano Lett.*, 8 (2008) 36–41.
- [34] T.R. Das, S. Patra, R. Madhuri, P.K. Sharma, Bismuth oxide decorated graphene oxide nanocomposites synthesized via sonochemical assisted hydrothermal method for adsorption of cationic organic dyes, *J. Colloid Interface Sci.*, 509 (2018) 82–93.
- [35] Z. Ji, C. Feng, X. Wu, Y. Li, L. Li, X. Liu, Composite of biomass and lead resistant *Aspergillus oryzae* for highly efficient aqueous phase Pb(II) adsorption, *Environ. Prog. Sustainable Energy*, 36 (2017) 1658–1666.
- [36] W. Zhang, Z. Yace, G. Yuvaraja, X. Jiao, Adsorption of Pb(II) ions from aqueous environment using eco-friendly chitosan schiff's base@Fe<sub>3</sub>O<sub>4</sub> (CSB@Fe<sub>3</sub>O<sub>4</sub>) as an adsorbent; kinetics, isotherm and thermodynamic studies, *Int. J. Biol. Macromol.*, 105 (2017) 422–430.
- [37] Q. Liu, F. Li, H. Lu, M. Li, J. Liu, S. Zhang, Q. Sun, L. Xiong, Enhanced dispersion stability and heavy metal ion adsorption capability of oxidized starch nanoparticles, *Food Chem.*, 242 (2018) 256–263.
- [38] A. Pal, K. Majumder, S. Sengupta, T. Das, A. Bandyopadhyay, Adsorption of soluble Pb(II) by a photocrosslinked polysaccharide hybrid: a swelling-adsorption correlation study, *Carbohydr. Polym.*, 177 (2017) 144–155.
- [39] Z. Zhou, Z.H. Xu, Q.J. Feng, D.H. Yao, J.G. Yu, D.S. Wang, S.Q. Lv, Y.F. Liu, N. Zhou, M.-e. Zhong, Effect of pyrolysis condition on the adsorption mechanism of lead, cadmium and copper on tobacco stem biochar, *J. Cleaner Prod.*, 187 (2018) 996–1005.
- [40] B. Wang, J.-L. Wen, S.-L. Sun, H.-M. Wang, S.-F. Wang, Q.-Y. Liu, A. Charlton, R.-C. Sun, Chemosynthesis and structural characterization of a novel lignin-based bio-sorbent and its strong adsorption for Pb(II), *Ind. Crops Prod.*, 108 (2017) 72–80.
- [41] A. Gil, M.J. Amiri, J. Abedi-Koupai, S. Eslamian, Adsorption/reduction of Hg(II) and Pb(II) from aqueous solutions by using bone ash/nZVI composite: effects of aging time, Fe loading quantity and co-existing ions, *Environ. Sci. Pollut. Res. Int.*, 23 (2018) 2814–2829.
- [42] Y. Huang, S.X. Li, J.H. Chen, X.L. Zhang, Y.P. Chen, Adsorption of Pb(II) on mesoporous activated carbons fabricated from water hyacinth using H<sub>2</sub>PO<sub>4</sub> activation: adsorption capacity, kinetic and isotherm studies, *Appl. Surf. Sci.*, 293 (2014) 160–168.
- [43] A.A. Yakout, R.H. El-Sokkary, M.A. Shreadah, O.G.A. Hamid, Cross-linked graphene oxide sheets via modified extracted cellulose with high metal adsorption, *Carbohydr. Polym.*, 172 (2017) 20–27.
- [44] G. Chen, K.J. Shah, L. Shi, P.-C. Chiang, Removal of Cd(II) and Pb(II) ions from aqueous solutions by synthetic mineral adsorbent: Performance and mechanisms, *Appl. Surf. Sci.*, 409 (2017) 296–305.
- [45] F.J. Sharahi, A. Shahbazi, Melamine-based dendrimer amine-modified magnetic nanoparticles as an efficient Pb(II) adsorbent for wastewater treatment: adsorption optimization by response surface methodology, *Chemosphere*, 189 (2017) 291–300.
- [46] Y. Qi, J. Wang, X. Wang, J.J. Cheng, Z. Wen, Selective adsorption of Pb(II) from aqueous solution using porous biosilica extracted from marine diatom biomass: properties and mechanism, *Appl. Surf. Sci.*, 396 (2017) 965–977.
- [47] K.Y. Foo, B.H. Hameed, Insights into the modeling of adsorption isotherm systems, *Chem. Eng. J.*, 156 (2010) 2–10.
- [48] H. Abdel-Samad, P.R. Watson, An XPS study of the adsorption of lead on goethite ( $\alpha$ -FeOOH), *Appl. Surf. Sci.*, 136 (1998) 46–54.